Received: 11 January 2024 | Accepted: 10 May 2024

DOI: 10.1002/ajb2.16376

Botany

RESEARCH ARTICLE

Estimates of late Early Cretaceous atmospheric CO_2 from Mongolia based on stomatal and isotopic analysis of *Pseudotorellia*

Xiaoqing Zhang[1,2] | Dana L. Royer[1] | Gongle Shi[2] | Niiden Ichinnorov[3] | Patrick S. Herendeen[4] | Peter R. Crane[5,6] | Fabiany Herrera[7]

[1]Department of Earth and Environmental Sciences, Wesleyan University, Middletown, CT 06459, USA

[2]State Key Laboratory of Palaeobiology and Stratigraphy, Nanjing Institute of Geology and Palaeontology, Chinese Academy of Sciences, Nanjing 210008, China

[3]Institute of Paleontology, Mongolian Academy of Sciences, Ulaanbaatar 15160, Mongolia

[4]Chicago Botanic Garden, Chicago, IL 60022, USA

[5]Oak Spring Garden Foundation, Oak Spring, Upperville, VA 20184, USA

[6]Yale School of Environment, Yale University, New Haven, CT 06511, USA

[7]Earth Sciences, Negaunee Integrative Research Center, Field Museum, Chicago, IL 60605, USA

Correspondence

Xiaoqing Zhang, Department of Earth and Environmental Sciences, Wesleyan University, 265 Church St., Middletown, CT 06459 USA.
Email: xzhang04@wesleyan.edu

Abstract

Premise: The Aptian–Albian (121.4–100.5 Ma) was a greenhouse period with global temperatures estimated as 10–15°C warmer than pre-industrial conditions, so it is surprising that the most reliable CO_2 estimates from this time are <1400 ppm. This low CO_2 during a warm period implies a very high Earth-system sensitivity in the range of 6 to 9°C per CO_2 doubling between the Aptian-Albian and today.

Methods: We applied a well-vetted paleo-CO_2 proxy based on leaf gas-exchange principles (Franks model) to two *Pseudotorellia* species from three stratigraphically similar samples at the Tevshiin Govi lignite mine in central Mongolia (~119.7–100.5 Ma).

Results: Our median estimated CO_2 concentration from the three respective samples was 2132, 2405, and 2770 ppm. The primary reason for the high estimated CO_2 but with relatively large uncertainties is the very low stomatal density in both species, where small variations propagate to large changes in estimated CO_2. Indeed, we found that at least 15 leaves are required before the aggregate estimated CO_2 approaches that of the full data set.

Conclusions: Our three CO_2 estimates all exceeded 2000 ppm, translating to an Earth-system sensitivity (~3–5°C/CO_2 doubling) that is more in keeping with the current understanding of the long-term climate system. Because of our large sample size, the directly measured inputs did not contribute much to the overall uncertainty in estimated CO_2; instead, the inferred inputs were responsible for most of the overall uncertainty and thus should be scrutinized for their value choices.

KEYWORDS

Albian, Aptian, fossil leaf cuticle, Ginkgoales, leaf-gas exchange model, paleoclimate, paleo-CO_2 proxy

Atmospheric CO_2 had a critical influence on ancient climates and terrestrial ecosystems (e.g., Montañez et al., 2011; Tierney et al., 2020; Westerhold et al., 2020; Hönisch et al., 2023). The Aptian-Albian (121.4–100.5 Ma) is widely understood as a greenhouse interval during the Cretaceous, with global temperatures estimated as 10–15°C warmer than pre-industrial conditions (e.g., Mills et al., 2019; Scotese et al., 2021). Earth-system sensitivity (ESS) describes the long-term rise in global mean surface temperature due to the radiative forcing associated with a doubling of CO_2 (Lunt et al., 2010; Rohling et al., 2012). The ESS values for the Phanerozoic, as inferred from geological studies, are typically in the 3–6°C range (Rohling et al., 2012; Royer, 2016; Krissansen-Totton and Catling, 2017; IPCC, 2021; Hönisch et al., 2023). Given these temperature constraints (~+12°C) and ESS (3–6°C per CO_2 doubling), one may expect 2–4 CO_2 doublings during the Aptian-Albian relative to the pre-industrial (i.e., 1120–4480 ppm).

CO_2 estimates for the Aptian-Albian based on stomatal frequencies, leaf gas-exchange, liverworts, paleosols, and phytoplankton proxies are relatively scarce and span a large range (225–2710 ppm) (Appendix S1: Table S1). Filtering these records for the most reliable estimates (following Hönisch et al., 2023 and the website https://paleo-co2.org/; "good quality" in Appendix S1: Table S1) reduces the total range (422–1340 ppm), but the central tendency is the same—unexpectedly low. This filtered CO_2 range implies an absolute minimum ESS value of 4.4°C averaged between the

Aptian-Albian and the present-day (10°C of warming divided by 2.3 CO_2 doublings associated with 1340 ppm CO_2); the mean expected ESS from the same filtered CO_2 data set is considerably higher (6–9°C).

The seeming mismatch between CO_2 and temperature estimates for the Aptian–Albian motivated us to generate new CO_2 estimates for this interval. Here, we reconstructed CO_2 based on two species of the leaf genus *Pseudotorellia* Florin, family Pseudotorelliaceae Krassilov within the Ginkgoales from three stratigraphically similar samples from the Tevshiin Govi lignite mine in central Mongolia (for background information on the site, see Shi et al., 2014, 2018). We used the leaf gas-exchange model of Franks et al. (2014) to convert measurements of stomatal size, stomatal frequency, and leaf $\delta^{13}C$ into paleoatmospheric CO_2 concentration. Our sampling design—combining a widely used proxy that is thought to be reliable (Hönisch et al., 2023; https://paleo-co2.org/) with the use of two species, several samples, and measurements from a large number (115) of leaves—maximizes the potential for robust results. We hypothesized that the CO_2 concentration was somewhere near the mid-range expectation of three doublings (2240 ppm) during the Aptian–Albian.

MATERIALS AND METHODS

Geological setting and flora

The leaves studied here are from the Tevshiin Govi lignite mine in central Mongolia, approximately 220 km south-southwest of Ulaanbaatar (45°58′54″ N, 106°07′12″ E; Leslie et al., 2013; Figure 1). The sediments are part of the Tevshiingovi Formation, which is considered Aptian–Albian (119.7–100.5 Ma) based on U/Pb ages from the base of the coeval Khukhteeg Formation that constrain the maximum age to 119.7 Ma and on biostratigraphy that accommodate an age as young as the end of the Albian (100.5 Ma) (Ichinnorov, 2003; Ichinnorov et al., 2012; Hasegawa et al., 2018; Heimhofer et al., 2022; Figure 1). Plant fossils are very abundant and exceptionally well preserved at the Tevshiin Govi lignite mine, including leaves with cuticle (Shi et al., 2014, 2018; Herrera et al., 2018), reproductive structures (Shi et al., 2014, 2016; Herrera et al., 2015, 2016, 2017a, 2017b, 2020; Bickner et al., 2024) and palynomorphs (Nichols et al., 2001, 2006; Ichinnorov, 2003; Ichinnorov et al., 2012; Shi et al., 2014). The lignite flora was deposited in a swamp-like environment with very little influx of detrital sediment. In one part of the Tevshiin Govi mine, four major lignite layers are intercalated between four channel deposits (Figure 1). We excavated lignite blocks from three stratigraphically similar samples from lignite #2 along the Tevshiin Govi lignite mine wall (PSH 261, PSH 292, PSH 417). The blocks were disaggregated with detergent, 3% v/v hydrogen peroxide, and deionized water. Because chemical treatments can affect $\delta^{13}C$ measurements (Barral et al., 2015), we measured one leaf (cut in half) with and without peroxide treatment and found an isotopic difference of 0.22‰, which propagates to a small change in estimated CO_2 (~2.6%). The lithological column was illustrated using SDAR package version 0.9-55 (Ortiz and Jaramillo, 2020).

We focused our CO_2 reconstruction work on two species of the genus *Pseudotorellia* (Kiritchkova and Nosova, 2009) that are both abundant and yield cuticles with excellent preservation of epidermal cellular structures: *Pseudotorellia resinosa* Shi, Herrera, Herendeen, Leslie, Ichinnorov, Takahashi et Crane and *Pseudotorellia palustris* Shi, Herrera, Herendeen, Leslie, Ichinnorov, Takahashi et Crane (Shi et al., 2018). These taxa, respectively, are inferred to be the leaves of the presumed ginkgophyte *Umaltolepis mongoliensis* (Herrera et al., 2017b; Shi et al., 2018) and the corystosperm *Doylea mongolica* (Shi et al., 2016, 2019, 2021).

Cuticle preparation

Complete to nearly complete leaves were first cut in half, with one half set aside for isotope analysis. The remaining half was cleared following standard practices (Dilcher, 1974; Wang, 2010; Liang et al., 2022). Fragments were soaked in deionized H_2O (dH_2O) for 1 h. Softened

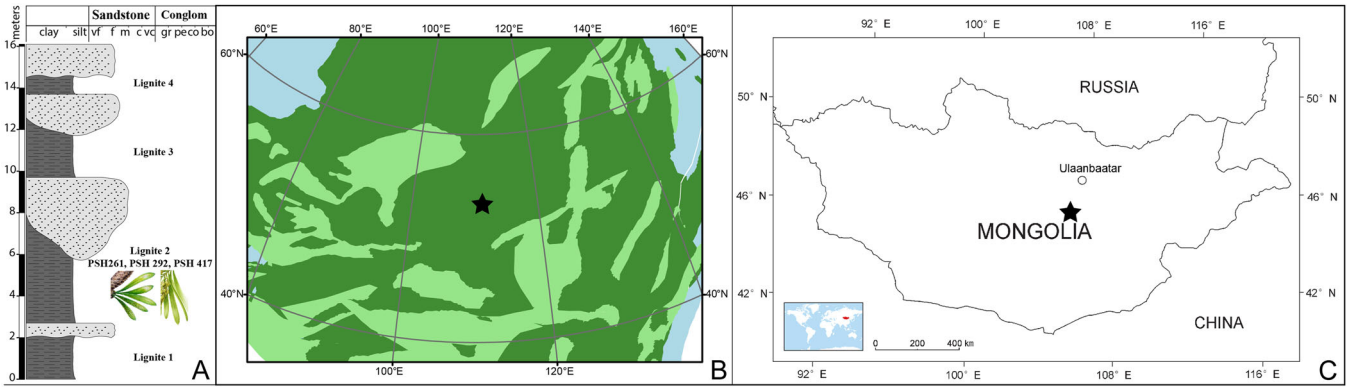

FIGURE 1 (A) Lithostratigraphy of locality. *Pseudotorellia* leaves from lignite #2 (samples PSH 261, PSH 292, PSH 417). (B) Paleogeography of region (derived from Matthews et al., 2016; Cao et al., 2017; Müller et al., 2018). Star icon represents Tevshiin Govi locality; dark green = lowlands; light green = highlands. (C) Modern geography of region.

leaf fragments were cut at the margin and then cleaned using dilute household bleach (c. 1% v/v NaClO solution). Once the leaves turned transparent (or light yellow), the reaction was immediately terminated by neutralizing with dH_2O, then the sample was transferred to a glass microscope slide. A fine dissecting needle was used to separate the leaf into the upper (adaxial) and lower (abaxial) sides, each containing one epidermis and part of the mesophyll tissues. They were then gently washed with dH_2O twice to remove loosened mesophyll tissue. All measurements were summarized by Zhang et al., 2024 (available at Dryad: https://datadryad.org/stash/dataset/doi:10.5061/dryad.g1jwstqzv). All specimens are archived in the paleobotanical collections of the Field Museum (collection numbers with the prefix PP).

Data analyses

Leaf cuticle measurements

Clean abaxial epidermises were observed with a Leica (Wetzlar, Germany) DMLB microscope and transmitted light and epifluorescence with mercury light and a 420–490 nm filter cube. Z-stack images of four focal planes were taken with a Jenoptik (Jena, Germany) Gryphax digital microscope camera and then integrated into a single composite image. We measured stomatal density mostly at 100× (field of view: 0.80 mm^2), but occasionally at 200× (field of view: 0.20 mm^2) when lower-quality preservation limited large fields of view. The stomata in both species appear randomly distributed (Figure 2A).

For each leaf fragment, we measured the length and width of 10 guard cells and their bounded stomatal pore. These images were taken at 400× and measured using ImageJ (Rasband, 1997). Both species of *Pseudotorellia* are hypostomatous and have sunken guard cells. *Pseudotorellia resinosa* possesses thickened subsidiary cells that partly overlap the underlying guard cells (Shi et al., 2018: fig. 16C–E). These thickened areas are prominent under both transmitted light (Figure 2B) and epifluorescence (Figure 2C) and comprise a smaller footprint than the underlying guard cells (see representative lines for guard cell length [gcl] and single guard cell width [sgw] in Figure 2). The overlapping thickened subsidiary cells can make the edge of guard cells unclear under transmitted light (Figure 2B); in this case, epifluorescence may give a better view.

Leaf $\delta^{13}C$ values

Bulk-leaf $\delta^{13}C$ values were measured at the Light Stable Isotope Mass Spec Lab at the Department of Geological Sciences of the University of Florida (Gainesville, FL, USA) using a Thermo Electron (Waltham, MA, USA) DeltaV Advantage isotope ratio mass spectrometer coupled with a ConFlo II interface linked to a Carlo Erba (Milan, Itay) NA 1500 CNHS Elemental Analyzer. After combustion in a quartz column at 1000°C in an oxygen-rich atmosphere, the sample gas was transported in a He carrier stream and passed through a hot reduction

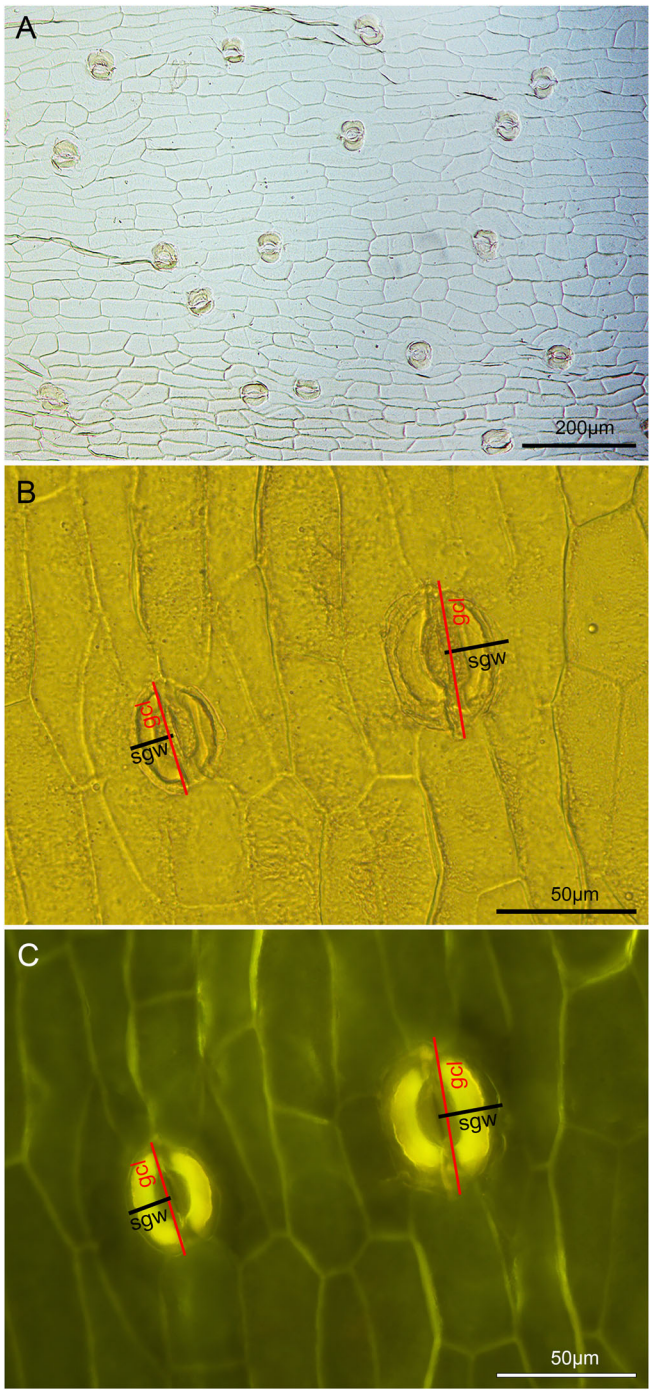

FIGURE 2 *Pseudotorellia resinosa* at (A) 10× magnification with transmitted light (specimen PP 61922) and at 40× magnification with (B) transmitted light and (C) epifluorescence (specimen PP 61941). Red lines are guard cell length (gcl); black lines are single guard cell width (sgw).

column (650°C) consisting of elemental copper to remove oxygen. The effluent stream then passed through a magnesium perchlorate trap to remove water followed by a 0.7-m GC column at 125°C to separate N_2 from CO_2. The sample gas next passed into a ConFlo II interface and into the inlet of a Thermo Electron Delta V Advantage isotope ratio mass spectrometer and was measured in continuous flow mode relative to the laboratory reference CO_2 gas. All carbon isotopic results are expressed in standard delta notation relative to Vienna Pee Dee Belemnite (VPDB). Instrument error across the multiple runs ranged from 0.01 to 0.19‰. We analyzed 36 samples in duplicate, with an average difference of 0.33‰ (0.06–1.03‰ range).

Leaf gas-exchange model

A well-vetted paleo-CO_2 proxy based on leaf gas-exchange principles (Franks et al., 2014; Royer et al., 2019) was used for paleo-CO_2 reconstruction. We used the R scripts of the Franks model v.2 (Kowalczyk et al., 2018) to carry out the calculations (see Appendix S1: Tables S2–S3 for input files formatted to run the model for the individual leaves and species means; see Appendix S1: Table S4 for definitions and units of all inputs). Given our comparatively large sample size (e.g., 42 *Pseudotorellia resinosa* leaves at PSH 261), we sought to test the sensitivity of estimated CO_2 to number of leaves and to variations in inputs from individual specimens. For the latter, the ranges reflected the variability across all plants in geologic time (following Maxbauer et al., 2014); we stress that these sensitivity tests are artificial because in the natural world a change in one input (e.g., stomatal density) will likely lead to a cascade of changes in other inputs (e.g., stomatal size), leading to a diminishment in the sensitivity. We thus emphasize the relative rankings of input sensitivities, not their exact quantitative implications.

Some of the inputs in the Franks model that cannot be measured directly can vary based on taxonomic affinity. One example is the leaf assimilation rate at a known CO_2 concentration, A_0. Franks et al. (2014) assigned default A_0 values of 12, 10, and 6 μmol m^{-2} s^{-1} to angiosperms, conifers, and other gymnosperms, respectively. Using these recommendations, we considered an A_0 value in the range of 6–10 μmol m^{-2} s^{-1} as most appropriate for *Pseudotorellia resinosa* and *P. palustris*, which we constrained further based on differences in vein density.

Vein density in living plants can correlate with leaf assimilation rate (Brodribb et al., 2010; Boyce and Zwieniecki, 2012; Sack et al., 2013; McElwain et al., 2016). However, we are hesitant to interpret these extant correlations quantitatively because they exhibit wide variance (e.g., $r^2 = 0.12$ [Sack et al., 2013]). Vein densities are higher in *Pseudotorellia palustris* than *P. resinosa* (28–40 vs. 16–18 veins per cm; Shi et al., 2018). Because both species have parallel venation, these density units can be converted to millimeters of vein length per square millimeter of leaf tissue (2.8–4.0 vs. 1.6–1.8 mm mm^{-2}). Based on these differences, we tentatively assigned an A_0 to the low end of our plausible range (6 μmol m^{-2} s^{-1}) for *P. resinosa* and the higher end of the range (10 μmol m^{-2} s^{-1}) for *P. palustris*.

For inputs that cannot be measured in fossils, Franks et al. (2014) recommended a 1σ uncertainty term of 5% of the mean value, which for A_0 would be 0.3 and 0.5 μmol m^{-2} s^{-1} respectively for *Pseudotorellia resinosa* and *P. palustris*. Recognizing the uncertain systematic position of both species among extant seed plants, we increased the uncertainty term to 1.0 μmol m^{-2} s^{-1} for both species and executed alternative runs assuming an A_0 of 6 and 10 μmol m^{-2} s^{-1} for both species.

For all other inferred inputs, we followed previous literature recommendations (Franks et al., 2014; Maxbauer et al., 2014; Kowalczyk et al., 2018; Royer et al., 2019; see Appendix S1: Table S3). For the $\delta^{13}C$ of atmospheric CO_2, we synthesized the predictions of Barral et al. (2017) for the 119.7–100.5 Ma interval (–5.5 ± 0.6‰ 1σ).

RESULTS

Stomatal measurements and leaf $\delta^{13}C$ values

The stomatal density of *Pseudotorellia resinosa* is very low, with mean densities of 13.4, 15.5, and 11.8 mm^{-2} in samples PSH 261, PSH 292, and PSH 417, respectively. The stomatal density of *P. palustris* is slightly higher (24.6 mm^{-2} at PSH 261). In both species, the stomates are comparatively small, with species-site means ranging from 19.2–22.9 μm for pore length and 42.9–47.7 μm for guard cell length. The site-mean leaf $\delta^{13}C$ of *P. resinosa* is similar for all three samples (–25.4, –24.9, and –24.7‰ for PSH 261, PSH 292, and PSH 417, respectively), but shifted slightly toward less-negative values in *P. palustris* (–22.8‰).

Estimates of CO_2

Our species-median estimated CO_2 concentrations from 42 leaves of *Pseudotorellia resinosa* and 26 leaves of *P. palustris* from the main sample (PSH 261) were both near 2000 ppm (thick black and red lines in Figure 3A). Combining the two species, we obtained a sample median of 2132 ppm (1229–3627 at 95% confidence; Figure 3A: purple and dashed lines). The estimated CO_2 from the other two samples broadly supported the estimates from PSH 261: The 24 *P. resinosa* leaves from PSH 292 yielded a median CO_2 concentration of 2405 ppm (1086–4854 ppm at 95% confidence; Figure 3B), and the 25 *P. resinosa* leaves from PSH 417 yielded a CO_2 concentration of 2770 ppm (1294–5977 ppm at 95% confidence; Figure 3C).

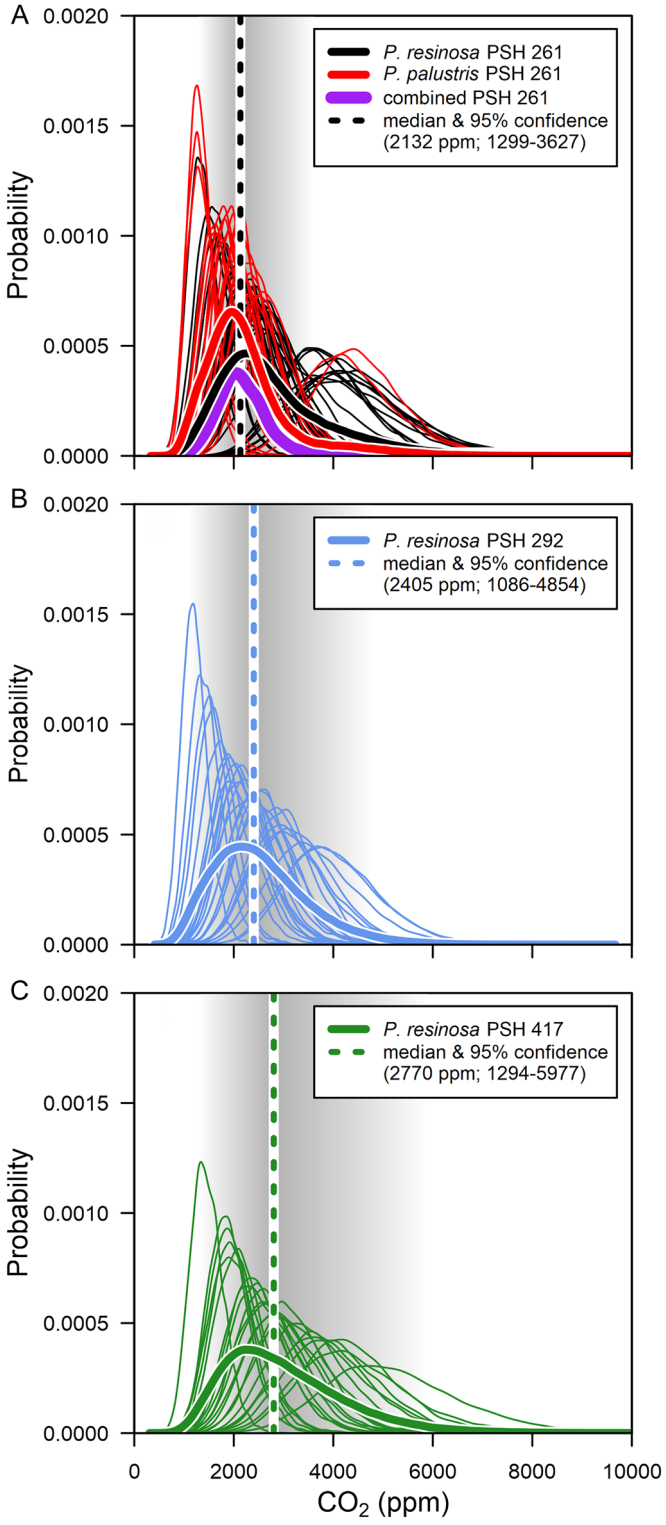

FIGURE 3 Estimated CO_2 concentration from late Early Cretaceous of Central Mongolia. Thin lines are probability density functions for individual leaves. Thick lines are the aggregate functions for species and samples; sample medians and 95% CIs are given in the legends and shown graphically with dashed lines and bounding gray envelopes. Estimates from the main sample, PSH 261 (A), are internally consistent between species and similar to estimates from the other two samples, PSH 292 (B) and PSH 417 (C).

If we assume an A_0 of 6 μmol m^{-2} s^{-1} for *P. palustris*, its median estimated CO_2 for PSH 261 drops to 1227 ppm (596–2966 ppm at 95% confidence), and the median for both species in the sample falls to 1614 ppm (Appendix S2: Figure S1). If we assume an A_0 of 10 μmol m^{-2} s^{-1} for *P. resinosa*, its median CO_2 for PSH 261 rises to 4227 ppm (2234–9059 ppm at 95% confidence), and the median for both species rises to 2751 ppm (Appendix S2: Figure S2A); the medians at PSH 292 and 417 also rise into the 4000 ppm range (Appendix S2: Figure S2B–C).

DISCUSSION

How many specimens are needed for a reliable CO_2 estimate?

A minimum threshold of sampling is needed to reconstruct CO_2 reliably from fossil leaves. An oft-cited threshold is five leaves, which is based on sensitivity tests of data sets comprising more than five leaves (e.g., Beerling and Royer, 2002; Slodownik et al., 2021). Our 42 *Pseudotorellia resinosa* leaves from PSH 261 provided the opportunity to test this threshold. We resampled one randomly selected leaf, then two leaves, and so forth, up to the full 42-leaf data set, then repeated this exercise 10,000 times at each level of subsampling. Figure 4 shows the pattern of estimated CO_2 for these repeated subsamples. Based on only five leaves, there is still significant variance in estimated CO_2. The black line in Figure 5 shows the same data but expressed as a coefficient of variation (mean divided by the SD). Compared to some other published data sets comprising >5 leaves, our fossils require a higher level of sampling to achieve equivalent reliability in estimated CO_2 (Figure 5). For example, to achieve the same level of reliability with five leaves for the other studies summarized in Figure 5, close to 15 *P. resinosa* leaves are required. This outcome motivated us to go back and process more leaves of *P. palustris* and *P. resinosa* in the other samples, so that we had a minimum of 24 leaves. We urge that, in future studies, data should be analyzed in a similar framework to guide decisions about adequate minimum level of sampling.

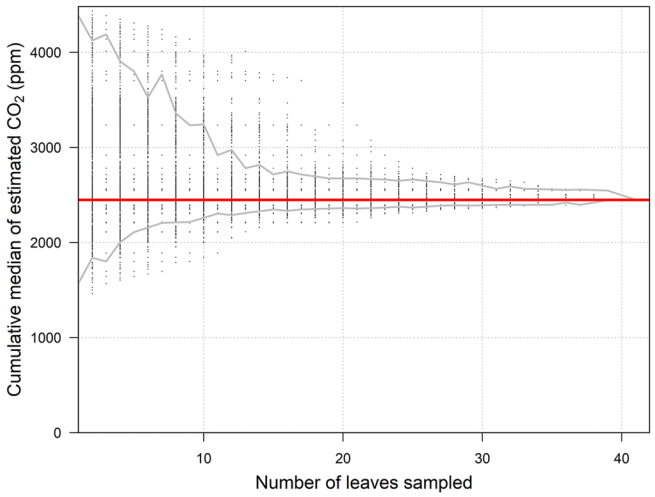

FIGURE 4 Cumulative median of estimated CO_2 relative to the number of leaves sampled for *Pseudotorellia resinosa* sample PSH 261. Small dots are individual CO_2 estimates based on randomized subsamples; gray envelope captures 95% of the individual runs. The horizontal red line is the estimated CO_2 when all 42 leaves are included.

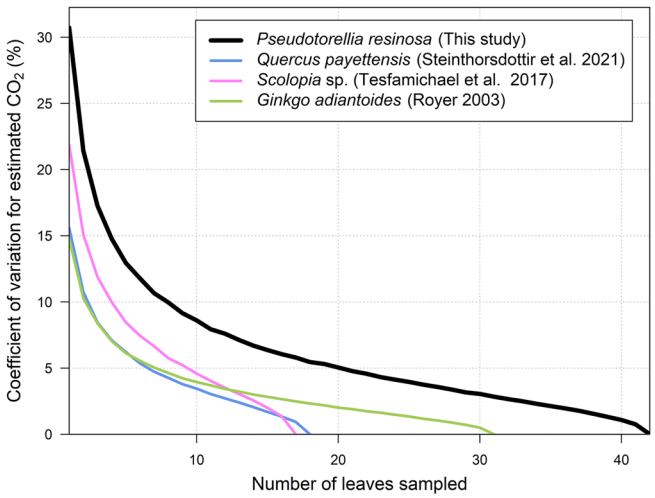

FIGURE 5 Coefficient of variation for the sensitivity analysis presented in Figure 4 (black line) for *Pseudotorellia resinosa* from PSH 261. This sensitivity is compared to other published studies using the Franks model (*Quercus* from Steinthorsdottir et al., 2021; *Scolopia* from Tesfamichael et al., 2017) and the stomatal index proxy (*Ginkgo* from Royer, 2003).

Sensitivity of key parameters for the Franks model

Because of the nonlinear mathematics of the Franks model, it can be difficult to know a priori how variations in individual inputs affect estimated CO_2. In other words, which inputs should we be most concerned about getting right? Figure 6 shows a sensitivity analysis for six key inputs, where the circles correspond to the mean measured (panels A–C) or inferred (panels D–F) values. Variations in stomatal density have the most effect on estimated CO_2 (Figure 6A), mostly because the mean values are so low (<25 mm^{-2}); variations above 50 mm^{-2} have little effect on estimated CO_2.

Of the inferred inputs, the ratio of operational to maximum stomatal conductance to CO_2 [$g_{c(op)}/g_{c(max)}$ or ζ or s4; Figure 6E] and the assimilation rate at a known CO_2 concentration (A_0; Figure 6F) are the most sensitive. This rank ordering is consistent with other sensitivity analyses (Maxbauer et al., 2014; Kowalczyk et al., 2018; Milligan et al., 2019) and underscores the importance of carefully considering their value choices. We acknowledge that the uncertainty regarding the

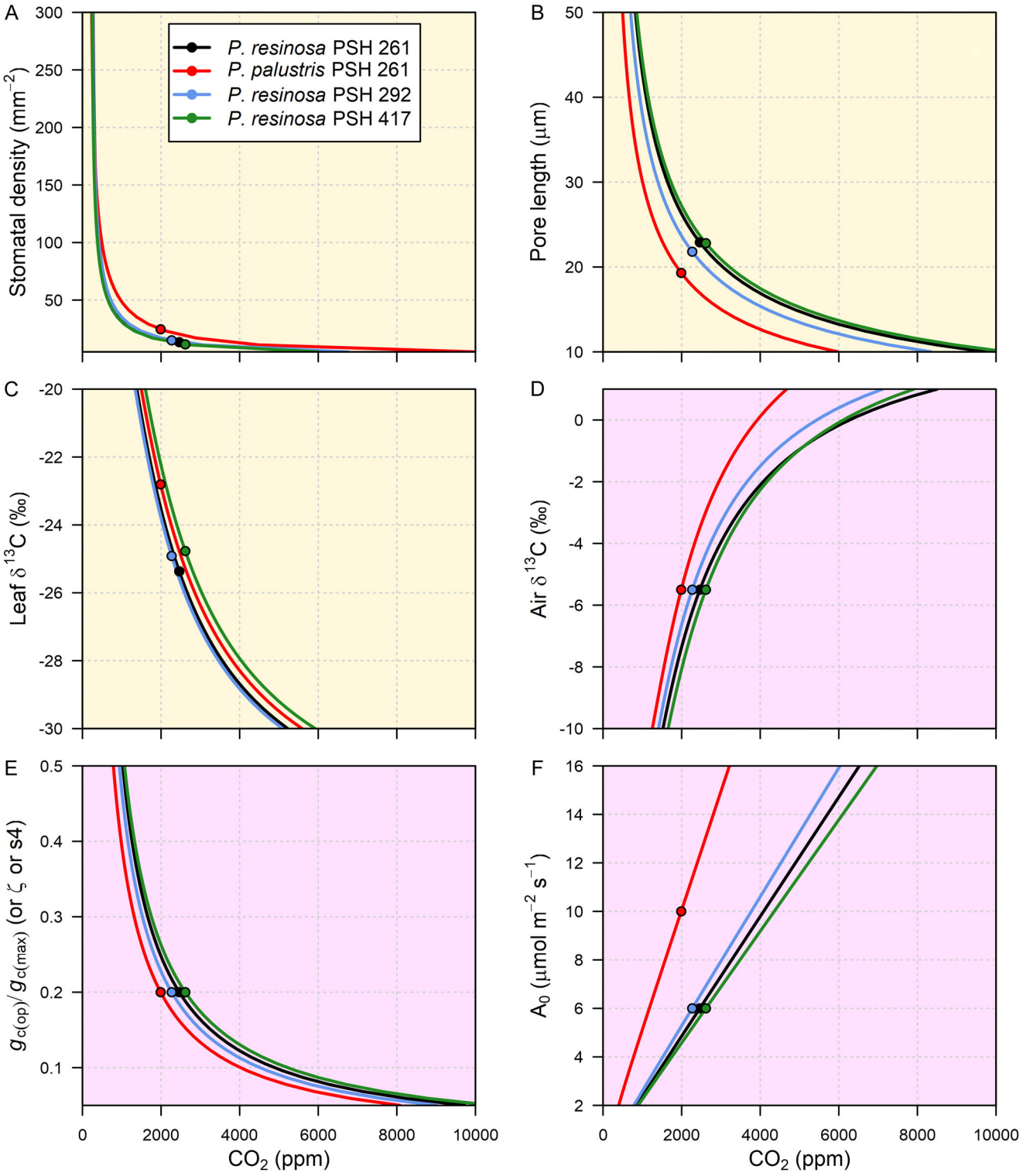

FIGURE 6 Sensitivity of individual inputs on estimated CO_2. The ranges correspond roughly to the ranges for vascular land plants or the environment (for air $\delta^{13}C$) across the Phanerozoic. The circles are the values used in our estimates. Panels A–C are measured inputs (yellow background); panels D–F are estimated inputs (pink background).

relationship of *Pseudotorellia palustris* and *P. resinosa* limits our ability to constrain A_0 (6–10 µmol m^{-2} s^{-1}), which in turn introduces considerable uncertainty in estimating CO_2 (Figure 6F; also compare Figure 3 to Appendix S2: Figures S1, S2). We note, however, that our preferred choice for A_0 in *P. palustris* (10 µmol m^{-2} s^{-1}), based on its relatively high vein density, leads to remarkably similar CO_2 estimates to those based on *P. resinosa* (Figure 4A).

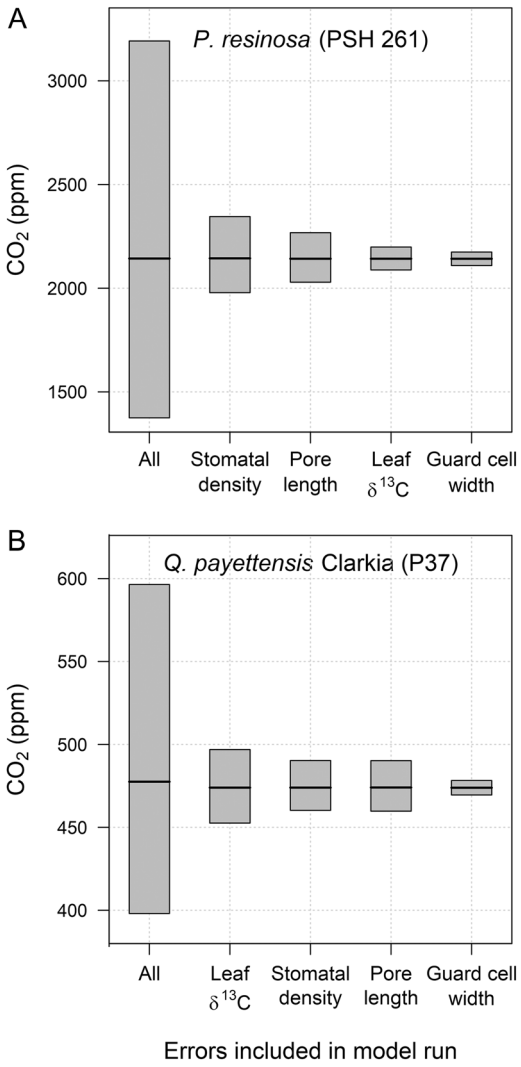

FIGURE 7 Contribution of individual measured inputs to the overall uncertainty in estimated CO_2. The four inputs with the largest contributions—ranked from largest to smallest—are shown along with the overall uncertainty. Middle lines are medians; height of bars correspond to 95% confidence. (A) *Pseudotorellia resinosa* at PSH 261 (this study); (B) *Quercus payettensis* from Steinthorsdottir et al. (2021).

Of the four directly measured inputs, uncertainty in stomatal density is the largest contributor to the overall uncertainty in estimated CO_2 (Figure 7A), which is not surprising given the sensitivity tests of Figure 6. A similar analysis of the published data of Steinthorsdottir et al. (2021) for *Quercus payettensis* finds a different rank order, with leaf $\delta^{13}C$ contributing the most uncertainty (Figure 7B); their measured stomatal densities are much higher (>800 mm^{-2}), so their variations propagate to less change in estimated CO_2.

We emphasize that the aggregate of all four measured inputs is a minority contributor to overall uncertainty in estimated CO_2 (compare "All" to the sum of the other four inputs in Figure 7). This underscores the importance of a large sample size; it is one element of the input uncertainties that the user has substantial control over. The inferred inputs, especially $g_{c(op)}/g_{c(max)}$ and A_0, contribute an outsized portion to the overall uncertainty.

Combination of low stomatal density and small stomatal size

Stomatal size and density determine the maximum stomatal conductance of CO_2 [$g_{c(max)}$] to the site of assimilation. Typically, size and density are anti-correlated across many living and fossil plants (Figure 8; Franks and Beerling, 2009), but not in our two species; size and (especially) density were low relative to most plants compiled by Franks and Beerling (2009) (black and red diamonds in Figure 8; Appendix S1: Table S5). This appears to be generally true with living and fossil ginkgo leaves, to which *Pseudotorellia* has generally been assumed to be related. Even under high CO_2 concentration, with lower stomatal density, they tend to retain smaller guard cells (yellow diamonds for fossil ginkgos and green circle for extant ginkgo in Figure 8). Both low density and small size contribute to a high estimated CO_2 (see also Figure 6A–B).

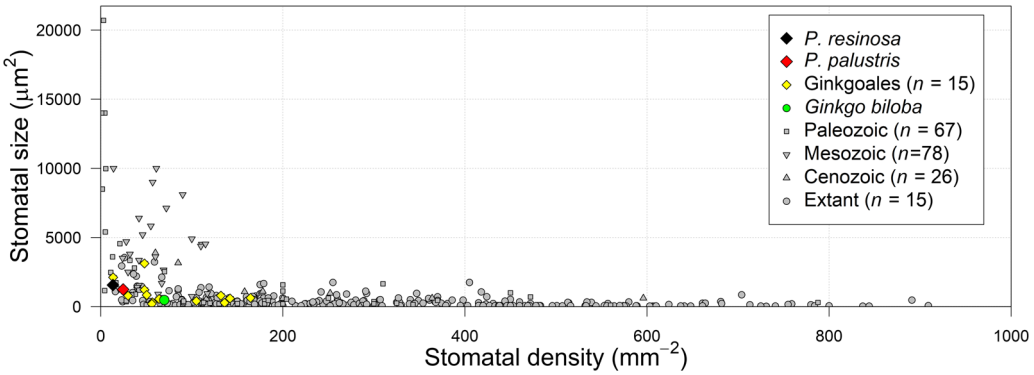

FIGURE 8 Relationship between stomatal density and guard cell size in the published literature (modified after Franks and Beerling, 2009). Black diamond: *Pseudotorellia resinosa* (this study); red diamond: *P. palustris* (this study); yellow diamonds: fossil Ginkgoales (additional data from Wu et al., 2016; Kowalczyk et al., 2018; Sun et al., 2018; Milligan et al., 2019; Zhou et al., 2020); green circle: extant *Ginkgo biloba* (Kowalczyk et al., 2018).

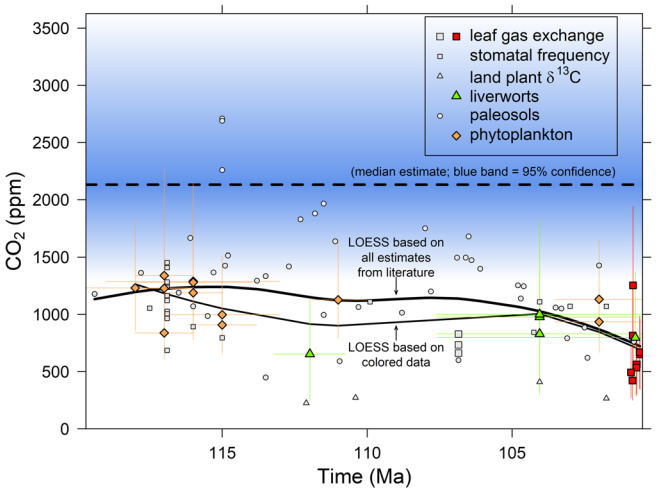

FIGURE 9 Published CO_2 estimates for the time interval constrained by our site (119.7–100.5 Ma). See Appendix S1: Table S1 for literature data. The colored symbols are the most reliable estimates (after paleo-CO2.org, Hönisch et al., 2023, and Steinthorsdottir et al., 2024). Two locally estimated scatterplot smoothing (LOESS) curves for the literature data are shown. For comparison, the black dashed line and blue band correspond to our median (2132 ppm) and 95% CI (1299–3627 ppm) for PSH 261.

Comparison with other CO_2 records

Our median estimated CO_2 for PSH 261 (2132 ppm) is higher than almost all published data for the age bracketed by our site (Figure 9). Among the subset of more reliable estimates (colored symbols in Figure 9; Appendix S1: Table S1), the mean is 926 ppm, and the maximum is 1340 ppm. There is a general trend toward lower CO_2 across our interval of interest (drop from ~1200 to ~700 ppm; see LOESS curves in Figure 9). Our median estimate is slightly less than three CO_2 doublings relative to a pre-industrial concentration of 280 ppm. This concentration is near the middle of the range predicted if one assumes a global mean surface temperature 12°C warmer than the pre-industrial as is widely accepted for the late Early Cretaceous (Mills et al., 2019; Scotese et al., 2021) and an ESS somewhere between 3 and 6°C per CO_2 doubling (Rohling et al., 2012; Royer, 2016; Krissansen-Totton and Catling, 2017; IPCC, 2021; Hönisch et al., 2023). Thus, our results are significant and are more in keeping with how we think Earth's climate responds over geologic time scales.

CONCLUSIONS

We analyzed two species of *Pseudotorellia* from the late Early Cretaceous Tevshiin Govi Formation in central Mongolia to reconstruct atmospheric CO_2 with a leaf-gas exchange model. Our median estimates from three samples (2132, 2405, and 2770 ppm) exceed almost all previously reported CO_2 estimates for the same period but are much more in-line with our current understanding of climate sensitivity. The very low stomatal densities necessitate a relatively large sample size to achieve stable and reliable CO_2 estimates (a minimum of 15 leaves per median estimate contrary to the commonly assumed minimum of five leaves). With these larger sample sizes, stomatal density and the other directly measured inputs do not contribute much to the overall uncertainty in estimated CO_2; instead, the inferred inputs, especially $g_{c(op)}/g_{c(max)}$ and A_0, are responsible for most of the overall uncertainty and thus should be scrutinized carefully for their value choices.

ACKNOWLEDGMENTS

We thank G. Tsolmon and L. Uranbileg for assistance with fieldwork in Mongolia, J. Curtis (University of Florida) for help with carbon isotope analyses, S. Gómez for assistance with lithological column and paleogeographic reconstruction in Figure 1, and M. Bickner and J. Bell Kaye for help picking fossil material. We thank Associate Editor Anne-Laure Decombeix and two anonymous reviewers for helpful advice and suggestions. This paper was supported by the National Science Foundation of USA (grant no. NSF 20-509) to D.L.R., the National Natural Science Foundation of China (grant no. NSFC 42202024) to X.Z., Natural Science Foundation of Jiangsu Province, China (grant no. BK20221160) to X.Z., and the National Geographic Society (grant no. EC-96755R-22) to F.H.

CONFLICT OF INTEREST STATEMENT

The authors declare they have no conflicts of interest.

DATA AVAILABILITY STATEMENT

Raw data of Cretaceous Mongolia leaf cuticle measurements from this study are available for download at Dryad: https://datadryad.org/stash/dataset/doi:10.5061/dryad.g1jwstqzv.

ORCID

Xiaoqing Zhang http://orcid.org/0009-0008-0797-9414
Dana L. Royer http://orcid.org/0000-0003-0976-953X
Gongle Shi http://orcid.org/0000-0003-3374-6637
Niiden Ichinnorov http://orcid.org/0000-0001-9044-5940
Patrick S. Herendeen http://orcid.org/0000-0003-2657-8671
Peter R. Crane http://orcid.org/0000-0003-4331-6948
Fabiany Herrera http://orcid.org/0000-0002-2412-672X

REFERENCES

Barral, A., C. Lécuyer, B. Gomez, F. Fourel, V. Daviero-Gomez. 2015. Effects of chemical preparation protocols on $\delta^{13}C$ values of plant fossil samples. *Palaeogeography, Palaeoclimatology, Palaeoecology* 438: 267–276.

Barral, A., B. Gomez, S. Legendre, and C. Lécuyer. 2017. Evolution of the carbon isotope composition of atmospheric CO_2 throughout the Cretaceous. *Palaeogeography, Palaeoclimatology, Palaeoecology* 471: 40–47.

Beerling, D. J., and D. L. Royer. 2002. Fossil plants as indicators of the Phanerozoic global carbon cycle. *Annual Reviews of Earth and Planetary Sciences* 30: 527–556.

Bickner M., F. Herrera, G. Shi, N. Ichinnorov, P. R. Crane, and P. S. Herendeen. 2024. *Mongolitria*: a new Early Cretaceous three-valved seed from East Asia. *American Journal of Botany* 111: e16268.

Boyce, C. K., and M. A. Zwieniecki. 2012. Leaf fossil record suggests limited influence of atmospheric CO_2 on terrestrial productivity prior to angiosperm evolution. *Proceedings of the National Academy of Sciences* 109: 10403–10408.

Brodribb, T. J., T. S. Feild. and L. Sack. 2010. Viewing leaf structure and evolution from a hydraulic perspective. *Functional Plant Biology* 37: 488.

Cao, W., S. Zahirovic, N. Flament, S. Williams, J. Golonka, and R. D. Müller. 2017. Improving global paleogeography since the late Paleozoic using paleobiology. *Biogeosciences* 14: 5425–5439.

Dilcher, D. L. 1974. Approaches to the identification of angiosperm leaf remains. *Botanical Review* 40: 1–157.

Franks, P. J., and D. J. Beerling. 2009. Maximum leaf conductance driven by CO_2 effects on stomatal size and density over geologic time. *Proceedings of the National Academy of Sciences, USA* 106: 10343–10347

Franks, P. J., D. L. Royer, D. J. Beerling, P. K. Van de Water, D. J. Cantrill, M. M. Barbour, and J. A. Berry. 2014. New constraints on atmospheric CO_2 concentration for the Phanerozoic. *Geophysical Research Letters* 41: 4685–4694.

Hasegawa, H., H. Ando, N. Hasebe, N. Ichinnorov, T. Ohta, T. Hasegawa, M. Yamamoto, et al. 2018. Depositional ages and characteristics of Middle–Upper Jurassic and Lower Cretaceous lacustrine deposits in southeastern Mongolia. *Island Arc* 27: e12243.

Heimhofer, U., H. Hasegawa, N. Ichinnorov, S. Flögel, S. Steinig, L. Zieger, and R. Littke. 2022. Early Cretaceous lignites from inner-continental Asia as a palaeoclimate archive. 11th International Cretaceous Symposium Warsaw, Abstract volume, 184–185.

Herrera, F., G. Shi, A. B. Leslie, P. Knopf, N. Ichinnorov, M. Takahashi, P. R. Crane, and P. S. Herendeen. 2015. A new voltzian seed cone from the Early Cretaceous of Mongolia and its implications for the evolution of ancient conifers. *International Journal of Plant Sciences* 176: 791–809.

Herrera, F., A. B. Leslie, G. Shi, P. Knopf, N. Ichinnorov, M. Takahashi, P. R. Crane, and P. S. Herendeen. 2016. New fossil Pinaceae from the Early Cretaceous of Mongolia. *Botany* 94: 885–915.

Herrera, F., G. Shi, N. Ichinnorov, M. Takahashi, E. V. Bugdaeva, P. S. Herendeen, et al. 2017b. The presumed ginkgophyte *Umaltolepis* has seed-bearing structures resembling those of Peltaspermales and Umkomasiales. *Proceedings of the National Academy of Sciences, USA* 114: E2385–E2391.

Herrera, F., G. Shi, P. Knopf, A. B. Leslie, N. Ichinnorov, M. Takahashi, P. R. Crane, and P. S. Herendeen. 2017a. Cupressaceae conifers from the Early Cretaceous of Mongolia. *International Journal of Plant Sciences* 178: 19–41.

Herrera, F., G. Shi, C. Mays, N. Ichinnorov, M. Takahashi, J. J. Bevitt, P. S. Herendeen, and P. R. Crane. 2020. Reconstructing *Krassilovia mongolica* supports recognition of a new and unusual group of Mesozoic conifers. *PLoS One* 15: e0226779.

Herrera, F., G. Shi, G. Tsolmon, N. Ichinnorov, M. Takahashi, P. R. Crane, and P. S. Herendeen. 2018. Exceptionally well-preserved Early Cretaceous leaves of Nilssoniopteris from central Mongolia. *Acta Palaeobotanica* 58: 135–157.

Hönisch B., D. L. Royer, D. O. Breecker, P. J. Polissar, G. J. Bowen, M. J. Henehan, Y. Cui, et al. 2023. Toward a Cenozoic history of atmospheric CO_2. *Science* 382: 6675.

Ichinnorov, N. 2003. Palynocomplex of the Lower Cretaceous sediments of Eastern Mongolia. *Mongolian Geoscientist* 22: 12–16.

Ichinnorov, N., L. Jargal, N. Odgerel, and A. Enkhtuya. 2012. Palynology and petrology characteristics of the Lower Cretaceous Tevshiin Gobi coal deposit, Mongolia. *In* M. Huh, H. J. Kim and J-y. Park [eds.], 11th Symposium on Mesozoic Terrestrial Ecosystems, August 15–18, 2012, Gwangju, Korea. Korea Dinosaur Research Center, Chonnam National University, Gwangju, Korea.

IPCC [Intergovernmental Panel on Climate Change]. 2021. Climate change 2021—The physical science basis: Working Group I contribution to the Sixth Assessment Report of the Intergovernmental Panel on Climate Change. Cambridge University Press, Cambridge, UK.

Kiritchkova, A. I., and N. V. Nosova. 2009. The genus *Pseudotorellia* Florin (Ginkgoales): taxonomic and stratigraphic aspects. *Stratigraphy and Geological Correlation* 17: 615–631.

Kowalczyk, J. B., D. L. Royer, I. M. Miller, C. W. Anderson, D. J. Beerling, P. J. Franks, M. Grein, et al. 2018. Multiple proxy estimates of atmospheric CO_2 from an early Paleocene rainforest. *Paleoceanography and Paleoclimatology* 33: 1427–1438.

Krissansen-Totton, J., and D. C. Catling. 2017. Constraining climate sensitivity and continental versus seafloor weathering using an inverse geological carbon cycle model. *Nature Communications* 8: 15423.

Leslie, A. B., I. Glasspool, P. S. Herendeen, N. Ichinnorov, P. Knopf, M. Takahashi, and P. R. Crane. 2013. Pinaceae-like reproductive morphology inSchizolepidopsis canicularissp. nov. from the Early Cretaceous (Aptian-Albian) of Mongolia. *American Journal of Botany* 100: 2426–2436.

Liang, J., Q. Leng, D. F. Höfig, G. Niu, L. Wang, D. L. Royer, K. Burke, et al. 2022. Constraining conifer physiological parameters in leaf gas-exchange models for ancient CO_2 reconstruction. *Global and Planetary Change* 209: 103737.

Lunt, D. J., A.M. Haywood, G.A. Schmidt, U. Salzmann, P. J. Valdes, and H. J. Dowsett. 2010. Earth system sensitivity inferred from Pliocene modelling and data. *Nature Geoscience* 3: 60–64.

Matthews, K. J., K. T. Maloney, S. Zahirovic, S. E. Williams, M. Seton, and R. D. Mü. 2016. Global plate boundary evolution and kinematics since the late Paleozoic. *Global and Planetary Change* 146: 226–250.

Maxbauer, D. P., D.L. Royer, and B. A. LePage. 2014. High Arctic forests during the middle Eocene supported by moderate levels of atmospheric CO_2. *Geology* 42: 1027–1030.

McElwain, J. C., I. Montañez, J. D. White, J. P. Wilson, and C. Yiotis. 2016. Was atmospheric CO_2 capped at 1000 ppm over the past 300 million years? *Palaeogeography, Palaeoclimatology, Palaeoecology* 441: 653–658.

Montañez, P. I., D. R. Norris, T. Algeo, A. M. Chandler, R. K. Johnson, J. M. Kennedy, V. D. Kent, et al. 2011. Understanding Earth's deep past: lessons for our climate future. National Academies Press, Washington, D.C., USA.

Milligan, J. N., D. L. Royer, P. J. Franks, G. R. Upchurch, and M. L. McKee. 2019. No evidence for a large atmospheric CO_2 spike across the Cretaceous-Paleogene boundary. *Geophysical Research Letters* 46: 3462–3472.

Mills, B. J. W., A. J. Krause, C. R. Scotese, D. J. Hill, G. A. Shields, T. M. Lenton. 2019. Modelling the long-term carbon cycle, atmospheric CO_2, and Earth surface temperature from late Neoproterozoic to present day. *Gondwana Research* 67: 172–186.

Müller, R. D., J. Cannon, X. Qin, R. J. Watson, M. Gurnis, S. Williams, T. Pfaffelmoser, et al. 2018. GPlates: Building a virtual Earth through deep time. *Geochemistry, Geophysics, Geosystems* 19: 2243–2261.

Nichols, D. J., M. Watabe, Y. Ichinnorov, and Y. Ariunchimeg. 2001. Preliminary report on the palynology of the Gobi Desert, Mongolia. *In* D. K. Goodman and R. T. Clarke [eds.], Proceedings of the IX International Palynological Congress, Houston, Texas, U.S.A., 1996, 131–138. American Association of Stratigraphic Palynologists Foundation, Dallas, TX, USA.

Nichols, D. J., M. Matsukawa, and M. Ito. 2006. Palynology and age of some Cretaceous nonmarine deposits in Mongolia and China. *Cretaceous Research* 27: 241–251.

Ortiz, J., and C. Jaramillo. 2020. SDAR: a toolkit for stratigraphic data analysis. R package version 0.9-55. Website: https://CRAN.R-project.org/package=SDAR

Rasband, W. S. 1997. ImageJ. U. S. National Institutes of Health, Bethesda, MD, USA. Website: https://imagej.nih.gov/ij/

Rohling, E. J., A. Sluijs, H. A. Dijkstra, P. Köhler, R. S. W. van de Wal, A. S. von der Heydt, D. J. Beerling, et al. 2012. Making sense of palaeoclimate sensitivity. *Nature* 491: 683–691.

Royer, D. L. 2003. Estimating latest Cretaceous and Tertiary atmospheric CO_2 concentration from stomatal indices. *In* S. L. Wing, P. D. Gingerich, B. Schmitz, and E. Thomas [eds.], Causes and

consequences of globally warm climates in the Early Paleogene, 79–93. Geological Society of America Special Paper 369. Geological Society of America, Boulder, CO, USA.

Royer, D. L. 2016. Climate sensitivity in the geologic past. *Annual Review of Earth and Planetary Sciences* 44: 277–293.

Royer, D. L., K. M. Moynihan, M. L. McKee, L. Londoño, and P. J. Franks. 2019. Sensitivity of a leaf gas-exchange model for estimating paleoatmospheric CO_2 concentration. *Climate of the Past* 15: 795–809.

Sack, L., C. Scoffoni, G. P. John, H. Poorter, C. M. Mason, R. Mendez-Alonzo, and L. A. Donovan. 2013. How do leaf veins influence the worldwide leaf economic spectrum? Review and synthesis. *Journal of Experimental Botany* 64: 4053–4080.

Scotese, C. R. H.J. Song, B. J. W. Mills, and D. G. van der Meer, 2021. Phanerozoic paleotemperatures: The earth's changing climate during the last 540 million years. *Earth-Science Reviews* 215: 103503.

Shi, G., P. R. Crane, P. S. Herendeen, N. Ichinnorov, M. Takahashi, and F. Herrera. 2019. Diversity and homologies of corystosperm seed-bearing structures from the Early Cretaceous of Mongolia. *Journal of Systematic Palaeontology* 17: 997–1029.

Shi, G., F. Herrera, P. S. Herendeen, G. C. Elizabeth, and P. R. Crane. 2021. Mesozoic cupules and the origin of the angiosperm second integument. *Nature* 594: 223–226.

Shi, G., F. Herrera, P. S. Herendeen, A. B. Leslie, N. Ichinnorov, M. Takahashi, and P. R. Crane. 2018. Leaves of *Podozamites* and *Pseudotorellia* from the Early Cretaceous of Mongolia: stomatal patterns and implications for relationships. *Journal of Systematic Palaeontology* 16: 111–137.

Shi, G., A. B. Leslie, P. S. Herendeen, F. Herrera, N. Ichinnorov, M. Takahashi, P. Knopf, and P. R. Crane. 2016. Early Cretaceous *Umkomasia* from Mongolia: implications for homology of corystosperm cupules. *New Phytologist* 210: 1418–1429.

Shi, G., A. B. Leslie, P. S. Herendeen, N. Ichinnorov, M. Takahashi, P. Knopf, and P. R. Crane. 2014. Whole-plant reconstruction and phylogenetic relationships of *Elatides zhoui* sp. nov. (Cupressaceae) from the Early Cretaceous of Mongolia. *International Journal of Plant Sciences* 175: 911–930.

Slodownik, M., V. Vajda, and M. Steinthorsdottir. 2021. Fossil seed fern *Lepidopteris ottonis* from Sweden records increasing CO_2 concentration during the end-Triassic extinction event. *Palaeogeography, Palaeoclimatology, Palaeoecology* 564: 110157.

Steinthorsdottir, M., H. K. Coxall, A. M. de Boer, M. Huber, N. Barbolini, C. D. Bradshaw, N. J. Burls, et al. 2021. The Miocene: the future of the past. *Paleoceanography and Paleoclimatology* 36: e2020PA004037.

Steinthorsdottir, M., I. P. Montañez, D. L. Royer, B. J. W. Mills, and B. Hönisch. 2024. Phanerozoic atmospheric CO_2 reconstructed with proxies and models: current understanding and future directions. Reference Module in Earth Systems and Environmental Sciences 2024. Elsevier, Amsterdam, Netherlands. Website: https://doi.org/10.1016/B978-0-323-99762-1.00074-7

Sun, C. L., X. Tan, D. L. Dilcher, H. Wang, Y. L. Na, T. Li, and Y. F. Li. 2018. Middle Jurassic *Ginkgo* leaves from the Daohugou area, Inner Mongolia, China and their implication for palaeo-CO_2 reconstruction. *Palaeoworld* 27: 467–481.

Tesfamichael, T., B. Jacobs, N. Tabor, L. Michel, E. Currano, M. Feseha, R. Barclay, and J. Kappelman, M. Schmitz. 2017. Settling the issue of "decoupling" between atmospheric carbon dioxide and global temperature: $[CO_2]_{atm}$ reconstructions across the warming Paleogene-Neogene divide. *Geology* 45: 999–1002

Tierney, J. E., C. J. Poulsen, P. I. Montañez, T. Bhattacharya, R. Feng, H. L. Ford, B. Hönisch, et al. 2020. Past climates inform our future. *Science* 370: 6517.

Wang, L. 2010. Morphology and anatomy of *Metasequoia* leaves and their environmental indicative values: evidence from the comparative studies of "living fossil" and fossils. Ph.D. dissertation, Nanjing Institute of Geology and Palaeontology, Chinese Academy of Sciences, Nanjing, China. [in Chinese with English summary].

Westerhold, T., N. Marwan, A. J. Drury, D. Liebrand, C. Agnini, E. Anagnostou, J. S. K. Barnet, et al. 2020. An astronomically dated record of Earth's climate and its predictability over the last 66 million years. *Science* 369: 1383–1387.

Wu, J. Y., S. T. Ding, Q. J. Li, B. Sun, and Y. D. Wang. 2016. Reconstructing paleoatmospheric CO_2 levels based on fossil *Ginkgoites* from the Upper Triassic and Middle Jurassic in Northwest China. *PalZ* 90: 377–387.

Zhang, X. Q., D. L. Royer, G. L. Shi, N. Ichinnorov, P. S. Herendeen, P. R. Crane, and F. Herrera. 2024. Data from: Estimates of late Early Cretaceous atmospheric CO2 from Mongolia based on stomatal and isotopic analysis of Pseudotorellia [dataset]. Dryad repository: https://doi.org/10.5061/dryad.g1jwstqzv

Zhou, N., Y. Wang, L. Ya, A. S. Porter, W. M. Kürschner, L. Li, N. Lu, and J. C. McElwain. 2020. An inter-comparison study of three stomatal-proxy methods for CO_2 reconstruction applied to early Jurassic Ginkgoales plants. *Palaeogeography, Palaeoclimatology, Palaeoecology* 542: 109547.

SUPPORTING INFORMATION

Additional supporting information can be found online in the Supporting Information section at the end of this article.

Figure S1. Estimated CO_2 concentration for PSH 261 assuming an A_0 value of 6 μmol m^{-2} s^{-1} for both *P. resinosa* and *P. palustris*.

Figure S2. Estimated CO_2 concentration for PSH 261 assuming an A_0 value of 10 μmol m^{-2} s^{-1} for both *P. resinosa* and *P. palustris*.

Table S1. Published CO_2 records during the Aptian to Albian. Level of quality follows paleo-CO_2.org.

Table S2. Franks model input for individual leaves.

Table S3. Franks model input for species means.

Table S4. Definitions of all abbreviation in Franks model input.

Table S5. Stomatal size.

How to cite this article: Zhang, X., D. L. Royer, G. Shi, N. Ichinnorov, P. S. Herendeen, P. R. Crane, and F. Herrera. 2024. Estimates of late Early Cretaceous atmospheric CO_2 from Mongolia based on stomatal and isotopic analysis of *Pseudotorellia*. *American Journal of Botany* 111(7): e16376. https://doi.org/10.1002/ajb2.16376